Confinement-Induced Ordering in Dewetting and Phase Separation of Polymer Blend Films

Xiao-Chun Chen, Hong-Min Li, Fei Fang, Yuan-Wei Wu, Mu Wang, Guo-Bin Ma, Yu-Qiang Ma, Da-Jun Shu, and Ru-Wen Peng*

Dewetting and phase separation of a thin polymer film over a homogeneous surface has been extensively investigated in recent decades. Research was driven either by scientific curiosity for general principles of rupture mechanisms[1–3] or by technical anticipation in finding out the conditions for stable lithographic resist layers.[4,5] Depending on the interfacial interactions, there are two possible rupture mechanisms of a polymer film: one occurs via nucleation of dry spots[6–8] and the other is by spontaneous amplifying the capillary waves caused by thermal fluctuation.[9–11] To demonstrate the effect of intermolecular interactions in the process, the influence of pattern scale and frequency on morphological evolution of the dewetting pattern of the thin polymer film can be tuned by topographically smooth, yet chemically inhomogeneous self-assembled monolayers.[12–15] In addition, physical modulations, such as periodic arrays of micro pillars,[16] stripes,[17,18] and holes[19] have also been introduced to the substrate surface in order to induce regular dewetting pattern. In previous studies, the common feature is that the polymer film remains physically continuous with the boundary extending to the edge of the sample. The chemical/topological inhomogeneity on the substrate merely plays a role of perturbation in the dewetting of polymer film. Yet it would be interesting to investigate pattern formation of polymer blend film on a surface with periodic lateral confinement (on a fishnet pattern, for example), where the boundaries of the polymer film move from the remote sample edge to the finite positions and hence affect the pattern formation process significantly.

It should also be mentioned that in conventional microfabrication process, ordered patterns are usually constructed by two different approaches. One is the top-down approach via conventional photolithography. The other is the bottom-up approach via self-assembling of smaller building blocks into larger structures. When the scale of lateral dimension of the system approaches the interaction range of the building blocks, which is expected to be the régime where bottom-up and top-down meet, a new ordering process may emerge, and the geometrical-confinement-induced self-organization should be visualized.

In this communication we demonstrate a unique process for the formation of ordered pattern in dewetting of polymer blend film on a periodically excavated silicon substrate. Once a lateral geometrical confinement is applied to the polymer blend film, the film may evolve to a perfectly ordered array of droplets when proper initial film thickness and interstitial separation of the holes on the substrate are selected. We suggest that our observation provides an example where interaction among the building blocks (the polymer droplets) and the interaction between the building block and the physical boundary of geometrical confinement work together to organize an ordered pattern. The principle revealed in this report is universal and should not be limited to polymer droplets only.

The annealed PS/PMMA blend film on the structured silicon substrate is illustrated in **Figure 1**a, where the squares are the excavated holes, and the circular bumps are the polymer droplets locating in the interstitial space among the holes. An AFM image of the droplets is shown in the inset. The droplets are nearly identical in shape. In contrast, on flat silicon substrate, with the same polymer film thickness, anneal temperature and anneal time, the droplets are random in both size and location, as shown in Figure 1b. Figure 1c illustrates the topography across the boundary of the excavated and the unexcavated regions. On the excavated substrate the droplets are well organized, whereas those on the flat substrate are random in location.

In situ AFM is applied to observe the dewetting and phase separation process of the polymer blend film. **Figure 2**a shows the topography of the film before anneal. Upon annealing, the film first shrinks slightly along the rims of the excavated holes, forming a narrow, evacuated region (Figure 2b). In the mean time the height of the polymer film fluctuates. The polymer film gradually evolves to the irregular islands via bicontinuous structures (Figure 2b–d). Further annealing makes the islands more rounded. Finally the circular droplets are formed (Figure 2e). Fast Fourier Transform (FFT) of the picture grabbed in between Figure 2b and c shows a well-defined isotropic ring, suggesting the existence of a characteristic length. In the anneal process, the neighboring droplets attract each other, approach gradually and coalesce to form a larger droplet, as marked by the circles in Figure 2e–i. During this process, smaller droplets are gradually annihilated by nearby larger ones, which is a coalescing and competition process. Eventually an array of uniform-sized droplets is accomplished in the interstitial regions of the excavated holes. Apparently this scenario is different from conventional

X.-C. Chen, Dr. H.-M. Li, F. Fang, Y.-W. Wu, Prof. M. Wang, Prof. G.-B. Ma, Prof. Y.-Q. Ma, Prof. D.-J. Shu, Prof. R.-W. Peng
National Laboratory of Solid State Microstructures & Department of Physics
Nanjing University
Nanjing 210093, China
E-mail: muwang@nju.edu.cn

DOI: 10.1002/adma.201200089

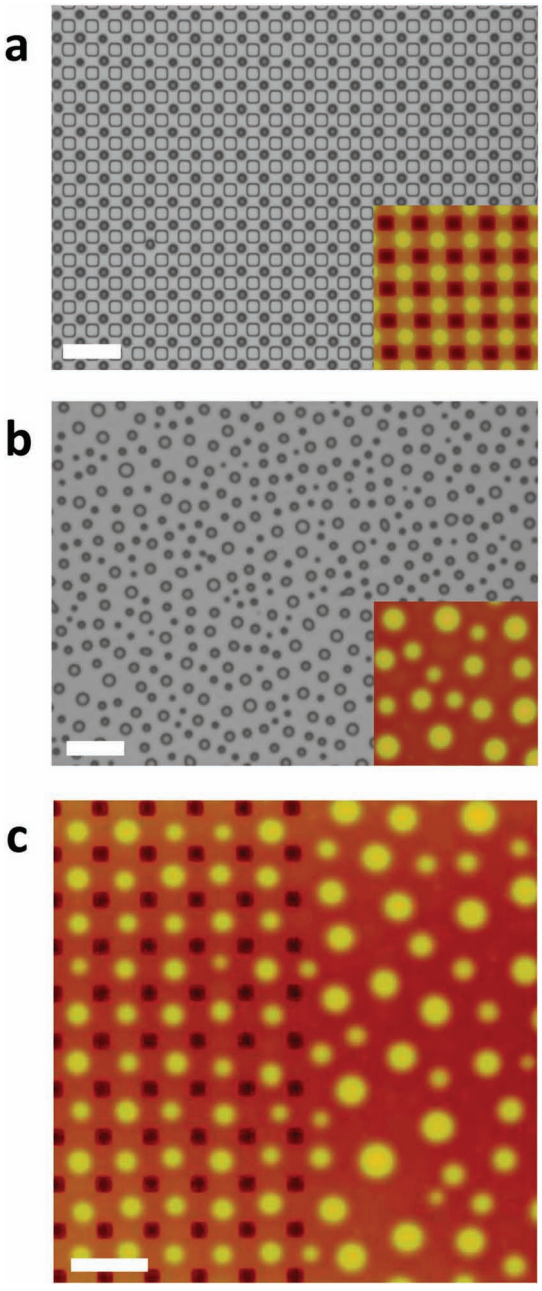

Figure 1. (a) Optical microscopy image of the annealed PS/PMMA blend film on the structured substrate. The lattice distance of the excavated holes on substrate is 4.0 μm. (b) Optical microscopy image of annealed PS/PMMA blend film on a substrate without any microstructure. In both (a) and (b), the insets are AFM images providing the detail topography. (c) AFM image at the boundary of the excavated region on substrate. The lattice parameter on the substrate is 6.0 μm. The scale bars represent 10 μm.

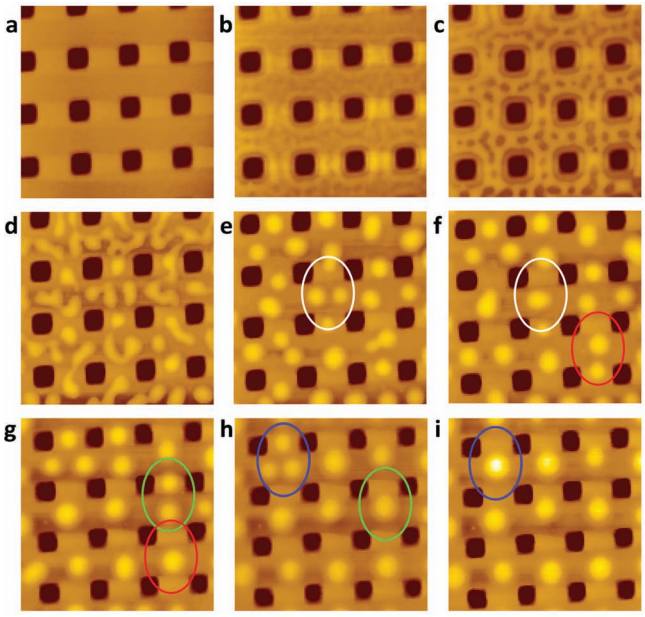

Figure 2. In situ AFM image of PS/PMMA blend film on the excavated substrate during the annealing process. The temperature is rapidly increased from room temperature to 150 °C and is stabilized at 150 °C. The vacuum is 2×10^{-5} Torr. (a) thin film before annealing, (b) the morphology observed at 120 °C. (c) the morphology observed at 150 °C. (d) the morphology after annealing for 10 min. (e) the morphology after annealing for 30 min. (f) the morphology after annealing for 1 hour. (g) the same area in 2 h. (h) the same area in 3 h, (i) the same area in 4 h. The circles with the same colour in (e)–(i) denote the drifting and coalescence of the droplets. The scan size is 20 μm for each frame.

Oswald ripening, where the smaller particle shrinks in size while the larger particle grows, yet their relative positions are anchored. This process is not a casting process either due to the self-adjusting and drifting of the positions of the droplets. It is noteworthy that the droplets do not appear on (or near) the edge of the holes, suggesting that there exists repulsive interaction between the droplet and the rim of the holes on the substrate.

By selective chemical dissolution we get the information of chemical components of the polymer droplets. **Figure 3**a shows the AFM image of the ordered droplets after annealing of the polymer blend film. The sample is then immersed in cyclohexane to selectively dissolve the PS phase. The remaining PMMA appears as a cofferdam-shaped ring, as illustrated in Figure 3b. This morphology is similar to previously reported pattern on a flat silicon substrate with native oxide layer,[20,21] indicating that the excavated holes on the substrate do not change the local phase separation process and the structure of each individual droplet. After dissolving the PS phase, we apply energy dispersive spectrometry (EDS) to map the distribution of PMMA on substrate. Figure 3c illustrates the topography of PMMA rings observed with SEM, and Figure 3d shows the carbon distribution over the same region. Although carbon signal can be detected over the whole substrate, the region corresponding to the cofferdam-shaped rings has apparently stronger intensity. This observation confirms that a very thin layer of PMMA covers the silicon substrate, and surrounding each PS kernel there is a cofferdam-shaped rim of PMMA.

Fourier transform of the topography of polymer droplets on a flat silicon substrate shows a homogeneous ring, which represents the average separation of the droplets, and can be used

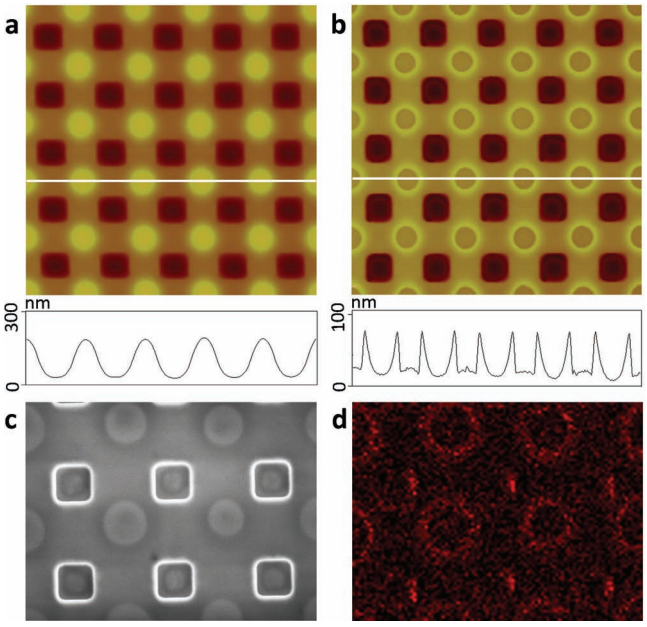

Figure 3. (a) Droplets of PS/PMMA formed at interstitial space of the excavated holes on substrate. (b) Surface morphology when PS has been selectively dissolved by cyclohexane. The remaining PMMA forms cofferdam-shaped rings. The graphs below (a) and (b) are the profile along the white line in (a) and (b), respectively. The scan size is 20 μm in (a)-(b). (c) is SEM topography and (d) is the mapping of energy-dispersive spectrometry (EDS) showing the distribution of carbon element in the same area.

as a characteristic length (λ_s) to describe the droplet assembly. Analysis of the data at different stage of the annealing process indicates that the characteristic length λ_s increases gradually and approaches to a stabilized value (details are shown in the Supporting Information). For larger λ_s, the diameter of the polymer droplets becomes larger, and droplet density decreases accordingly. We measure the stabilized annealed pattern of polymer blend film with different initial film thickness with the same surface patterning on the substrate. It turns out when the film thickness is so thin that its λ_s is much smaller than the lattice parameter of the hole array on the substrate, the droplets are random in both size and location, and are scattered on the stripe bounded by the excavated holes (**Figure 4**a). When the film is very thick that its λ_s becomes larger than the lattice parameter of the hole array, the droplet becomes much larger, and no spatial ordering is observed either (Figure 4c). Only when the film thickness is correctly selected that its λ_s is comparable to the lattice parameter of the holes, the ordered droplet array is achieved, as illustrated in Figure 4b.

To verify this scaling relation further, we investigate the scenario that the film thickness is fixed (consequently λ_s is determined), yet the lattice parameter of the excavated holes varies (Figure 4d–f). When the lattice parameter of the holes on the substrate is 6.0 μm, which is smaller than λ_s (here λ_s equals to 8.25 μm, see the Supporting Information for detail), the droplets do not follow the structure on the substrate surface. Instead, they form a random pattern. When the lattice parameter of the holes becomes 10.0 μm, which is larger than λ_s, the droplets cannot be efficiently confined by the boundaries either. Only

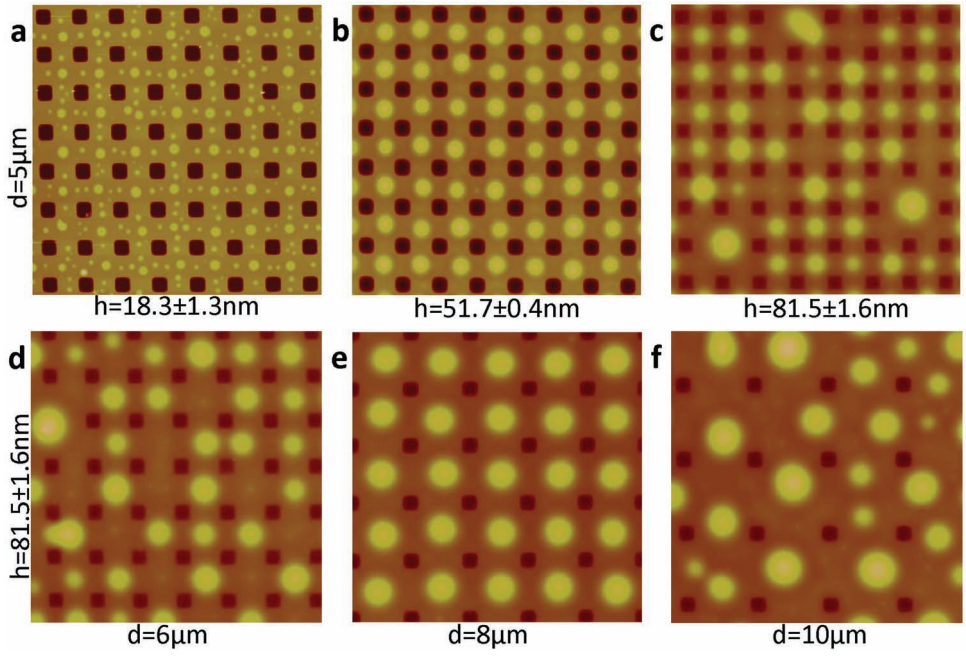

Figure 4. AFM images to show the dependence of the droplet distribution on film thickness and interstitial separation of the holes on the substrate. The anneal temperature and time are fixed at 150 °C for 48 h. The first row: the lattice parameter of the excavated holes is 5 μm, while the initial film thickness varies. (a) 18.3 nm; (b) 51.7 nm; (c) 81.5 nm. The second row: the film thickness is fixed as 81.5 nm, yet lattice parameter of the excavated hole array varies. (d) 6 μm; (e) 8 μm; and (f) 10 μm. The scan size is 40 μm for each frame.

when the interstitial separation is selected as 8.0 μm, which is comparable to λ_s, an ordered pattern is realized (Figure 4e). Figure 4 suggests that there exists a scaling relation between the film thickness and the lattice parameter of the holes on the substrate in order to generate an ordered pattern.

The pattern formation process described above can be understood as follows. By spin-coating, a layer of PS/PMMA blend film is formed on the interstitial strips of the patterned substrate (Figure 2a). Dewetting and phase separation occur upon anneal, and separated islands are formed, as illustrated in Figure 2b–d. It is noteworthy that on the interstitial stripe bounded by the excavated holes, PMMA exists not only adjacent to the PS kernel, but on the rest of the stripe area as well, forming a wettable layer extending to the rims of the excavated holes. In the vicinity of the rim of excavated holes, PMMA layer possesses a convex surface geometry. Adjacent the PS phase, by considering the interfacial energies of PS-air, PS-PMMA, PMMA-air and PMMA-silicon substrate, one may find that the energy-favorable configuration is that the PS phase protrudes from the PMMA layer with a hydrophilic meniscus, and PMMA forms a cofferdam pattern around the PS phase.[19] It is the local surface geometry that decides the nature of capillary interactions of the polymer droplets and the edge of the excavated holes. In annealing process, PS droplets protrude from PMMA layer, attract and coalesce with the neighboring ones. At the same time, repulsive interaction between the edge of the holes and the PS droplet confines the droplet. These interactions work jointly and form an ordered droplet array.

Quantitatively the capillary interaction between the particles floating on a surface has been reviewed by Kralchevsky and Nagayam.[22,23] The geometrical topography of the interface determines the nature of interaction. The meniscus slope angle ψ is used to characterize the surface property:[22] $\sin(\psi) > 0$ corresponds to the hydrophilic scenario and $\sin(\psi) < 0$ corresponds to the hydrophobic one. According to Ref. [22], the nature of capillary interaction between two floating objects is determined by $\sin(\psi_1)\cdot\sin(\psi_2)$, where ψ_1 and ψ_2 are the meniscus slope angles for objects 1 and 2, respectively. For two PS droplets floating on PMMA, ψ_1 and ψ_2 possess the same sign, $\sin(\psi_1)\cdot\sin(\psi_2) > 0$, so the capillary force between the droplets is attractive; for the interaction of a PS droplet and the rim of the excavated hole, ψ_1 and ψ_h possess the opposite sign, so $\sin(\psi_1)\cdot\sin(\psi_h) < 0$, indicating that the capillary force between the PS droplet and the rim of the hole is repulsive (detail analysis can be found in the Supporting Information). This means that the nature of the interaction simply depends on the shape of the geometrical meniscus around the objects.

Now we consider the scenario that a PS droplet appears near the center of the interstitial space bounded by excavated square holes. Based on the above discussions, the rims of the micro holes apply a repulsive force on the PS droplet. For simplicity, we consider a single droplet floating in between two straight, infinitely long rims separated by a distance of 2*L*, as illustrated in **Figure 5**. Suppose the profile of PMMA thin film between two parallel rims is $f(x)$, which can be approximately expressed as

$$f(x) = \sqrt{\frac{a}{L}(L^2 - x^2)}, \text{ with } a^2 = \frac{A}{6\pi\gamma} \quad (1)$$

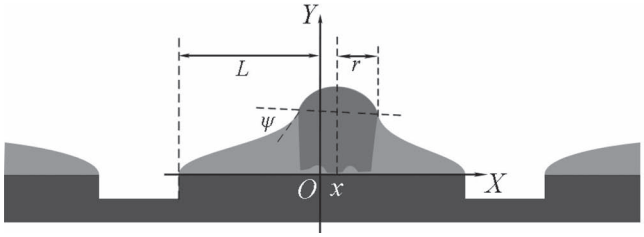

Figure 5. Schematic (not to scale) of a PS droplet close to the center of the interstitial region of two micro holes on the patterned substrate.

(details are available in the Supporting Information). For small droplet we ignore the force originated from hydrostatic pressure. The lateral capillary force acting on PS droplet is calculated by integrating the PMMA-air interfacial tension σ along the contact line (accurate to the linear term of x),

$$F_x = -\frac{2\pi r}{\sqrt{L^2 - r^2}}\sqrt{\frac{a}{L}}\sigma\sin\psi\ x - \ldots \approx -kx \quad (2)$$

where σ is the surface tension of PMMA-air interface, r is the radius of three phase contact circle, $k = \frac{2\pi r}{\sqrt{L^2 - r^2}}\sqrt{\frac{a}{L}}\sigma\sin\psi > 0$. Equation (2) clearly shows that the PS droplet trapped near the center of the interstitial region feels a spring-like restoring force, which keeps the droplet in the center of the interstitial region and stabilizes the regular array of the droplets.

Understanding and controlling the self-assembly process remains a challenging task. Our experiments provide an example that the interaction among the building blocks and the interaction between the building block and the physical boundaries of geometrical confinement cooperate jointly to organize an ordered pattern. The principle revealed in this process, i.e., controlling the capillary interactions through interfacial curvature design, is a universal one and is not limited to polymer droplets only. Technically, assembling polymer blend droplets into a regular array may inspire new applications such as efficient photodiodes and photovoltaic devices.[24–26] Once the polymer film is deposited in a laterally confined space, the periodically imposed boundaries on the substrate will contribute to the self-organization process. We suggest that this confinement-induced-ordering effect manifests a low-cost and convenient approach to generate polymer microstructures over a large area.

Experimental Section

Solution of polymer blend of polystyrene (PS) and poly(methylmethacrylate) (PMMA) was prepared by dissolving PS [Mw = 9.58 kg/mol, Mw/Mn = 1.03, Fluka] and PMMA [Mw = 9.98 kg/mol, Mw/Mn = 1.03, Fluka] in toluene with weight ratio 1:1. The PS/PMMA blend film was spin-coated on a structured silicon substrate, on which the excavated hole array was fabricated by photolithography. Each excavated hole had a lateral size 2 μm, and the depth was 500 nm. The lattice parameter of the array could be selected in the range of 4–10 μm. Before spin-coating, the substrate was ultrasonically cleaned in ethanol and acetone solution. The thickness of blend polymer films depended on the spin rate and the concentration of polymer blend solution, and was controlled in the range of 10–100 nm. The film thickness was measured by an ellipsometer (GES-5, Sopra). The polymer blend film was annealed in a vacuum oven at 150 °C for 48 h. The morphology of the annealed

sample was observed with optical microscope (D4000m, Leica) and atomic force microscope (AFM) (Nanoscope IIIa). To investigate the pattern evolution in dewetting and phase separation process, annealing of the polymer blend film was also observed in situ with a high-vacuum AFM (SPI 300HV, Seiko) at 150 °C and 2.0×10^{-5} Torr.

Supporting Information

Supporting Information is available from the Wiley Online Library or from the author.

Acknowledgements

This work was supported by the State Key Program for Basic Research from MOST of China (Grant No. 2010CB630705 and 2012CB921502), NSF of China (Grant No. 50972057, 11034005, & 61077023), and partly by Jiangsu Province (Grant No. BK2008012).

Received: January 8, 2012
Published online: April 12, 2012

[1] J. Koplik, J. R. Banavar, *Phys. Rev. Lett.* **2000**, *84*, 4401.
[2] J. Becker, G. Grun, R. Seemann, H. Mantz, K. Jacobs, K. R. Mecke, R. Blossey, *Nat. Mater.* **2003**, *2*, 59.
[3] H. I. Kim, C. Mathew Mate, K. A. Hannibal, S. S. Perry, *Phys. Rev. Lett.* **1999**, *82*, 3496.
[4] E. Schaffer, T. Thurn-Albrencht, T. P. Russell, U. Steiner, *Nature* **2000**, *403*, 874.
[5] L. Chen, L. Zhuang, P. Deshpande, S. Chou, *Langmuir* **2005**, *21*, 818.
[6] G. Reiter, *Phys. Rev. Lett.* **1992**, *68*, 75.
[7] K. Jacobs, S. Herminghaus, K. R. Mecke, *Langmuir* **1998**, *14*, 965.
[8] R. Seemann, S. Herminghaus, K. Jacobs, *Phys. Rev. Lett.* **2001**, *87*, 196101.
[9] R. Xie, A. Karim, J. F. Douglas, C. C. Han, R. A. Weiss, *Phys. Rev. Lett.* **1998**, *81*, 1251.
[10] E. Ruckenstein, R. K. Jain, *J. Chem. Soc. Faraday Trans. II* **1974**, *70*, 132.
[11] M. Sferrazza, M. Heppenstall-Butler, R. Cubitt, D. Bucknall, J. Webster, R. A. L. Jones, *Phys. Rev. Lett.* **1998**, *81*, 5173.
[12] A. Sehgal, V. Ferreiro, J. F. Douglas, E. J. Amis, A. Karim, *Langmuir* **2002**, *18*, 7041.
[13] M. Boltau, S. Walheim, J. Mlynek, G. Krausch, U. Steiner, *Nature* **1998**, *391*, 877.
[14] A. Karim, J. F. Douglas, B. P. Lee, S. C. Glotzer, J. A. Rogers, R. J. Jackman, E. J. Amis, G. M. Whitesides, *Phys. Rev. E* **1998**, *57*, R6273.
[15] D. Bandyopadhyay, A. Sharma, *J. Phys. Chem. C* **2010**, *114*, 2237.
[16] R. Mukherjee, D. Bandyopadhyay, A. Sharma, *Soft Matter* **2008**, *4*, 2086.
[17] R. Mukherjee, M. Gonuguntla, A. Sharma, *J. Nanosci. Nanotechnol.* **2007**, *7*, 2069.
[18] B. Z. Newby, R. J. Composto, *Phys. Rev. Lett.* **2001**, *87*, 098302.
[19] R. Xing, C. Luo, Z. Wang, Y. Han, *Polymer* **2007**, *48*, 3574.
[20] M. Harris, G. Appel, H. Ade, *Macromolecules* **2003**, *36*, 3307.
[21] Y. Li, Y. Yang, F. Yu, L. Dong, *J. Polymer Sci. B* **2006**, *44*, 9.
[22] P. A. Kralchevsky, K. Nagayama, *Adv. Colloid Interface Sci.* **2000**, *85*, 145.
[23] K. D. Danov, P. A. Kralchevsky, *Adv. Colloid Interface Sci.* **2010**, *154*, 91.
[24] J. J. M. Halls, C. A. Walsh, N. C. Greenham, E. A. Marseglia, R. H. Friend, S. C. Moratti, A. B. Holmes, *Nature* **2002**, *376*, 498.
[25] P. Peumans, S. Uchida, S. R. Forrest, *Nature* **2003**, *425*, 158.
[26] A. C. Morteani, A. S. Dhoot, J. S. Kim, C. Silva, N. C. Greenham, C. Murphy, E. Moons, S. Cina, J. H. Burroughes, R. H. Friend, *Adv. Mater.* **2003**, *15*, 1708.